Paper No.
2358

NACE INTERNATIONAL CORROSION 2013 CONFERENCE & EXPO

Effect of Calcium on the Formation and Protectiveness of Iron Carbonate Layer in CO_2 Corrosion

Saba Navabzadeh Esmaeely, Yoon-Seok Choi, David Young and Srdjan Nesic
Institute for Corrosion and Multiphase Technology,
Department of Chemical and Biomolecular Engineering,
Ohio University
Ohio, 45701
USA

ABSTRACT

Among the known options in carbon capture and storage (CCS), the injection and storage of CO_2 in deep saline aquifers has the potential to cause casing corrosion due to the direct contact between injected CO_2 and the saline aquifer, containing highly concentrated aqueous salts such as NaCl and $CaCl_2$. Thus, in the present study, the effect of Ca^{2+} on the CO_2 corrosion behavior of mild steel was investigated in simulated saline aquifer environments (1 wt.% NaCl, 80°C, pH 6.6) with different concentrations of Ca^{2+} (10, 100, 1,000 and 10,000 ppm). Electrochemical methods (open circuit potential (OCP) and linear polarization resistance (LPR) measurements) were used to measure the corrosion rate. Surface analysis techniques (scanning electron microscope (SEM), X-ray spectroscopy (EDS) and X-ray diffraction (XRD)), were used to characterize the morphology and identity of the corrosion products. The results show that with low concentrations of Ca^{2+} (10 and 100 ppm), the corrosion rate decreased with time due to the formation of protective $FeCO_3$ and/or $Fe_xCa_yCO_3$ ($x + y = 1$). However, the presence of high concentrations of Ca^{2+} (1,000 and 10,000 ppm) resulted in the change of corrosion product from protective $FeCO_3$ to non-protective $CaCO_3$, and an increasing corrosion rate with time. While the general corrosion rate was high for both 1,000 and 10,000 ppm Ca^{2+}, surface analysis data revealed a different steel surface morphology with pitting observed in the presence of 10,000 ppm Ca^{2+}.

Key words: $FeCO_3$, $CaCO_3$, Ca^{2+}, Fe^{2+}, localized corrosion, carbon capture and storage

INTRODUCTION

The threat of global climate change has become one of the most serious concerns of the 21st century. Major research efforts are underway to understand how it occurs and to develop ways to mitigate its impact on the environment. Carbon dioxide (CO_2) is known as one of the major contributors to greenhouse gas emissions, which have been hypothesized to lead to global warming. Since CO_2 emission is directly proportional to fossil fuel consumption, the capturing and subsequent geologic storage of CO_2 is a candidate technology for controlling its emission.[1] The carbon capture and storage (CCS) process contains three stages: CO_2 capture at its generation source (coal or gas fired power plant, refinery, syngas unit, cement works or some other industrial process), transportation to the geologic storage site (usually by pipeline transmission) followed by injection into geologic host reservoirs. [2]

Among the known options in CCS, injection and storage of CO_2 in deep saline aquifers has the potential to cause casing corrosion due to the direct contact between injected CO_2 and the saline aquifer with highly concentrated aqueous salts such as NaCl and $CaCl_2$. Corrosion rates of casing steel are highly dependent on the formation of iron carbonate ($FeCO_3$) in CO_2/saline aquifer environments. Brine species such as Ca^{2+}, which can form carbonate layers/scales, are very important in corrosion studies as they can compete with Fe^{2+} in the formation of carbonates. Therefore, there is a possibility of changing the $FeCO_3$ morphology, composition and protectiveness in such environments, and in turn, this can affect general and localized corrosion behavior of casing steel.

Little has been reported on the effect of Ca^{2+} on corrosion in the literature, with findings often appearing contradictory. Zhao, *et al*.,[3,4] claimed that corrosion rate decreased in the "short term" in the presence of Ca^{2+} and Mg^{2+}, but there was no special difference in "long term exposure". Ding, *et al*., reported the corrosion rate increased with an increase in the Ca^{2+} concentration. [5] Jiang, *et al*., reported pitting associated with $CaCl_2$. They claimed that while Cl^- caused pitting the presence of Ca^{2+} postponed the initiation of the pitting. [6] Ren, *et. al,* [7] as well as Zhu, *et al.,*[8] reported pitting with reference to the presence of Cl^- in $CaCl_2$ containing electrolytes. Gao, *et al.,* [9] reported pitting in conjunction with the formation of $Fe_xCa_yCO_3$ and $Fe_x(Mg,Ca)_yCO_3$ ($x+y=1$) on the steel surface. A broader review of the literature indicates that Cl^- ions are often associated with pitting; however the role of overall water chemistry, and in particularly Ca^{2+} ions, is generally not clear. In many instances some of the key parameters are not measured or reported, for example the pH of the aqueous solution is often "unknown" making any discussion of the results unconvincing. In CO_2 corrosion of mild steel, only higher pH is associated with formation of protective $FeCO_3$ layers and therefore any influence of Ca^{2+} concentration must be analyzed in the context of the overall water chemistry effects.

Thus, the objective of the present study is to evaluate the effect of Ca^{2+} on the CO_2 corrosion behavior of mild steel in simulated saline aquifer environments related to the injection and storage of CO_2, by conducting well controlled and thoroughly qualified experiments.

EXPERIMENTAL SETUP AND PROCEDURE

Experiments were conducted in a 2 liter glass cell using a three-electrode setup. In each experiment, three flat specimens made from AISI(1) 1018 mild steel [UNS G10180] with an exposed area of 5.4 cm^2 were used for electrochemical measurement and for surface analysis. Prior to insertion, the specimens were wet-polished with silicon carbide (SiC) paper, down to 600 grit, and rinsed with isopropyl alcohol in an ultrasonic bath and dried.

(1) American Iron and Steel Institute, 25 Massachusetts Avenue, NW Suite 800 | Washington, DC 20001

Table 1 and Table 2 show the test matrix and test conditions, respectively. The glass cell was filled with 2 liters of 1 wt.% NaCl electrolyte (prepared with deionized water). The solution was stirred with a magnetic stirrer and the temperature was set to 80°C, CO_2 gas was continuously purged through the solution. The solution pH was adjusted to 6.6 by addition of a deoxygenated 1.0 M sodium hydroxide solution. After the pH stabilized, the magnetic stir bar was stopped and samples were inserted into the glass cell.

The corrosion behavior was monitored by electrochemical methods: OCP and LPR measurements. Samples from all experiments were characterized by X-ray diffraction (XRD), scanning electron microscopy (SEM), energy dispersive X-ray spectroscopy (EDS) and infinite focus microscopy (IFM) to investigate the effect of Ca^{2+} on the morphology and composition of the corrosion product layer. The Ca^{2+} concentration was measured using inductively coupled plasma (ICP) spectroscopy. Analyses for the Fe^{2+} concentration were performed with a UV-Vis spectrophotometer.

At the end of each experiment and after completion of the corrosion product surface analysis, one sample from each experiment was treated with Clarke solution according to ASTM[(2)] G1 to remove the corrosion product layer and scan the underlying metal surface.[10]

Table 1 - Test Matrix

Parameters	Conditions
Total Pressure	0.1 MPa
pCO_2	0.05 MPa
Temperature	80°C
Solution	1 wt.% NaCl
pH	6.6
Flow condition	Stagnant
Steel	G10180

Table 2 – Test Conditions

Test condition #	Initial concentrations of Fe^{2+} and Ca^{2+}
1	10 ppm Fe^{2+}
2	10 ppm Fe^{2+} + 10 ppm Ca^{2+}
3	10 ppm Fe^{2+} + 100 ppm Ca^{2+}
4	10 ppm Fe^{2+} + 1,000 ppm Ca^{2+}
5	10 ppm Fe^{2+} + 10,000 ppm Ca^{2+}

RESULTS

Figure 1 shows the variations of OCP and corrosion rate with time for each experiment condition. As shown in Figure 1 (a), the corrosion rate decreased with time for the low initial Ca^{2+} concentration conditions. This indicates that a protective $FeCO_3$ layer was formed on the steel surface according to:

$$Fe^{2+}\ (aq.) + H_2CO_3\ (aq.) \rightarrow FeCO_3\ (s.) + 2\ H^+\ (aq.) \quad (1)$$

When a $FeCO_3$ layer forms on the mild steel surface, it can slow down corrosion by presenting a diffusion barrier for the species involved in the process, and by blocking (covering) a portion of the steel surface and preventing the underlying steel from undergoing further oxidative dissolution.[11, 12]

[(2)] American Society for Testing and Materials, 100 Barr Harbor Drive, PO Box C700, West Conshohocken, PA 19428-2959

For the low initial Ca^{2+} concentration conditions (0, 10 and 100 ppm), the formation of a protective $FeCO_3$ layer apparently occurred without significant interference by Ca^{2+} ions. However, the corrosion behavior of mild steel with higher initial Ca^{2+} concentrations of 1,000ppm and 10,000ppm was different. The corrosion rate did not decrease with time, which is likely due to the lack of formation of a protective $FeCO_3$ layer on the steel surface. At this stage it can be hypothesized that this was caused by a lower pH, seen in experiments with higher initial Ca^{2+} concentrations, as shown in Figure 2 (a). Note that precipitation of $CaCO_3$ in aqueous CO_2 solutions will lead to acidification, as the equilibrium pH is approached:

$$Ca^{2+}\ (aq.) + H_2CO_3\ (aq.) \rightarrow CaCO_3\ (s.) + 2\ H^+\ (aq.) \qquad (2)$$

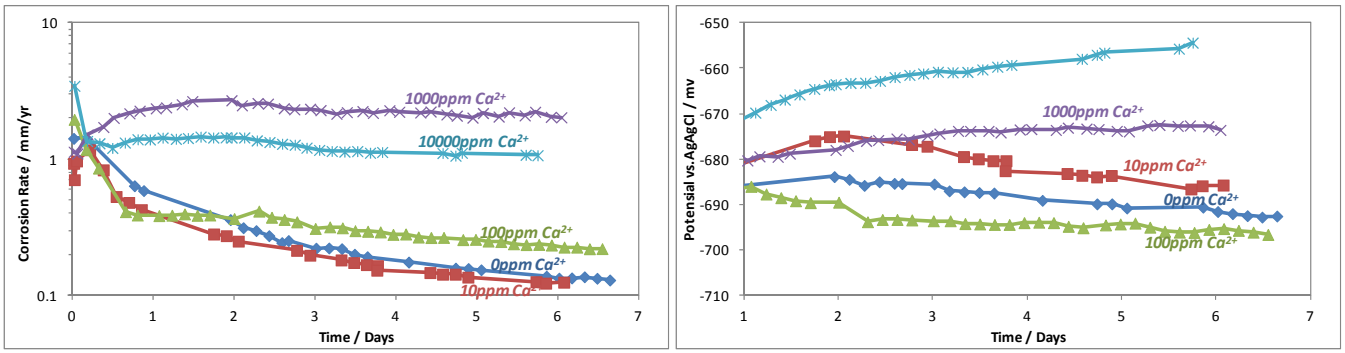

(a) (b)

Figure 1: Variations of (a) corrosion rate and (b) open circuit potential, for mild steel exposed to a simulated brine with different initial concentrations of Ca^{2+} at 80°C and pCO_2 of 0.05 MPa with 10ppm Fe^{2+}.

To illustrate this, Figure 2 (b) shows the variation of $FeCO_3$ saturation degree with time. The saturation degree (S) was calculated by Equation (3), based on the measured values of pH and Fe^{2+} concentration. The CO_3^{2-} concentration was calculated using a simple equilibrium model for aqueous CO_2 species.[13]

$$S_{FeCO_3} = \frac{[Fe^{2+}]*[CO_3^{2-}]}{K_{SP,FeCO_3}} \qquad (3)$$

The $K_{sp,FeCO3}$ is the solubility product of $FeCO_3$ calculated as:[14]

$$LogK_{SP,FeCO_3} = -59.3498 - 0.041377*T - \frac{2.11963}{T} + 24.5724Log(t) + 2.518*I^{0.5} - 0.6578*I \qquad (4)$$

As shown in Figure 2 (b), the experiments with lower Ca^{2+} concentrations remained highly supersaturated with respect to $FeCO_3$ during the whole experiment, leading to steady precipitation of protective $FeCO_3$. The experiment with initial Ca^{2+} concentration of 1,000 ppm was also supersaturated with respect to $FeCO_3$, while at the initial Ca^{2+} concentration of 10,000 ppm, the rapid precipitation of $CaCO_3$ made the solution under-saturated with respect to $FeCO_3$, making it impossible for protective $FeCO_3$ layer to form.

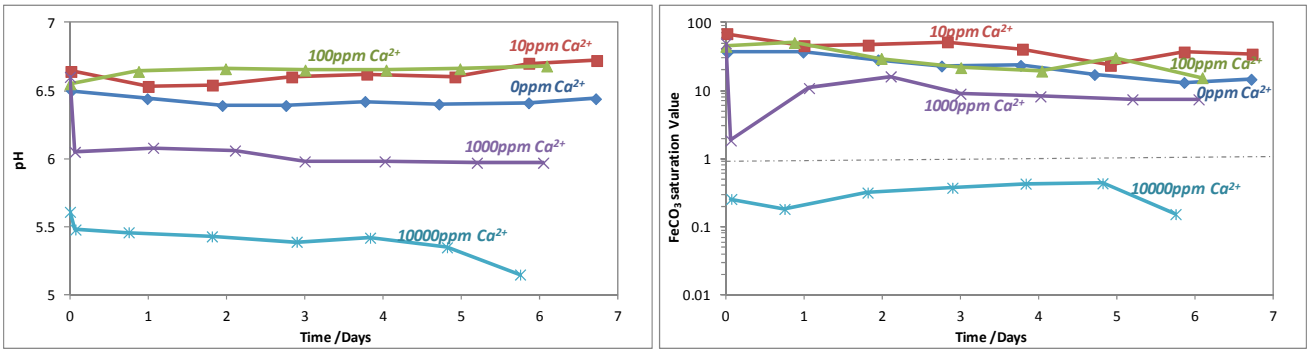

(a) (b)

Figure 2: Variations of (a) pH and (b) saturation degree of $FeCO_3$, for mild steel exposed to a simulated brine with different/varying concentrations of Ca^{2+} at 80°C and pCO_2 of 0.05 MPa with 10ppm Fe^{2+}.

In order to explain this behavior in more detail, let us now focus on the experiment with initial Ca^{2+} concentration of 1,000 ppm. The measured variations of Fe^{2+} concentration and Ca^{2+} concentration with time are plotted in Figure 3 (a). The concentration of Ca^{2+} decreased steadily due to precipitation of $CaCO_3$. The Fe^{2+} concentration initially decreased due to precipitation of $FeCO_3$ from a supersaturated solution and then as the saturation level was approached, the Fe^{2+} concentration increased due to the high general corrosion rate, see Figure 1 (a).

The corresponding saturation degrees with respect to $CaCO_3$ and $FeCO_3$ *versus* time are given in Figure 3 (b). There, based on the measured pH and Ca^{2+}, the saturation degree with respect to $CaCO_3$ was calculated according to:

$$S_{CaCO_3} = \frac{[Ca^{2+}]*[CO_3^{2-}]}{K_{SP,CaCO_3}} \quad (5)$$

Where $K_{sp,CaCO3}$ is the solubility product of $CaCO_3$ calculated as: [15]

$$LogK_{SP,CaCO_3} = -1228.732 - 0.2994444*T + \frac{35512.75}{T} + 485.818LogT \quad (6)$$

As is shown in Figure 3, due to a very high initial concentration of Ca^{2+}, the aqueous solution was initially highly supersaturated with respect to $CaCO_3$. This led to precipitation of $CaCO_3$ reducing the level of saturation. As the $CaCO_3$ supersaturation level approached 10, the driving force for $CaCO_3$ precipitation decreased and the concentration of calcium changed very slowly. At the same time the Fe^{2+} concentration initially decreased much more rapidly than the Ca^{2+} concentration, even if the initial level of supersaturation with respect to $FeCO_3$ was much lower than that of $CaCO_3$, pointing to a much faster kinetics. As the level of $FeCO_3$ supersaturation fell below 10, the kinetics of $FeCO_3$ precipitation decreased, while at the same time the corrosion rate remained unchanged, see Figure 1 (a), which led to an increase in Fe^{2+} concentration over time.

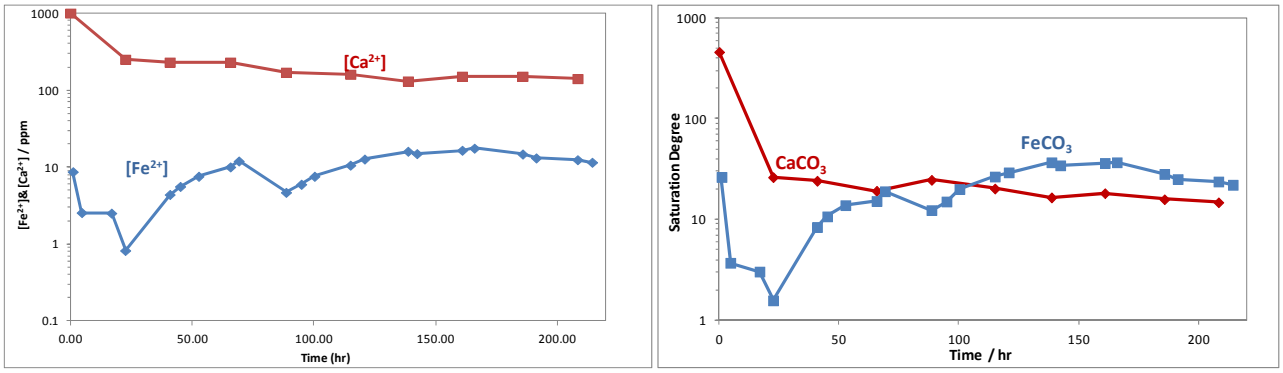

(a) (b)

Figure 3: (a) Fe^{2+} and Ca^{2+} concentrations and (b) $CaCO_3$ and $FeCO_3$ saturation degree for the initial 1,000 ppm [Ca^{2+}] system *versus* time at 80°C and pCO_2 of 0.05 MPa with 10ppm Fe^{2+}.

Figure 4 shows the SEM images of specimens from electrolytes with 0ppm Ca^{2+}, 10ppm Ca^{2+}, 100ppm Ca^{2+}, 1,000ppm Ca^{2+} and 10,000ppm Ca^{2+}. The analyses for the experiments with 0, 10 and 100 ppm Ca^{2+} shows scattered crystals of $FeCO_3$ on the surface, corrosion product crystal morphologies did not appreciably change at these relatively low Ca^{2+} concentrations. However, at higher Ca^{2+} concentration, as shown in Figure 4 (d) and (e) for 1,000 ppm [Ca^{2+}] and 10,000 ppm [Ca^{2+}], respectively, the crystal morphologies at the surface significantly changed due to the presence of Ca^{2+}. In the experiment with 1,000 ppm Ca^{2+} the crystals were mostly elongated. For the electrolyte with 10,000 ppm Ca^{2+}, the surface was covered with a dense, intergrown layer of scale rather than being comprised of relatively discrete crystals.

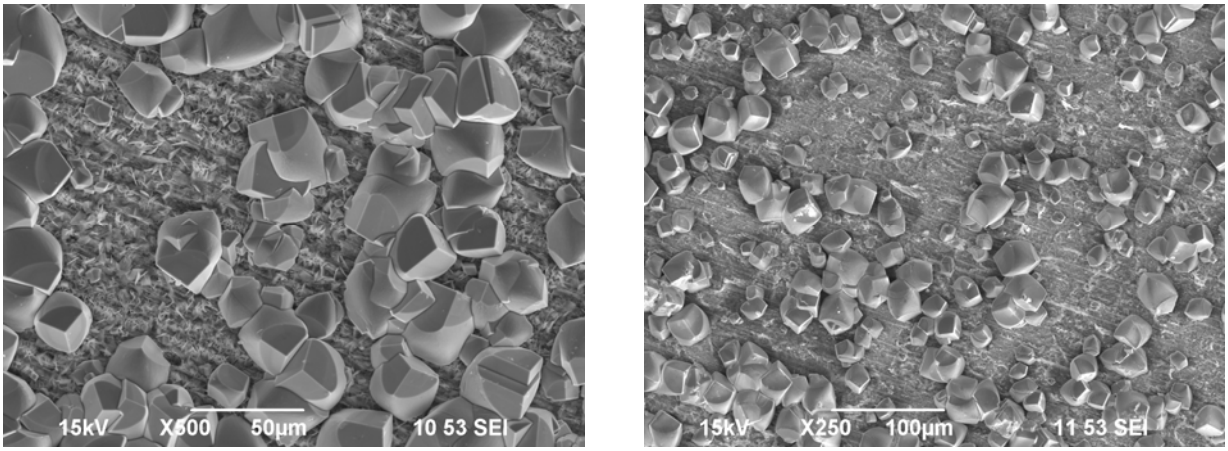

(a) (b)

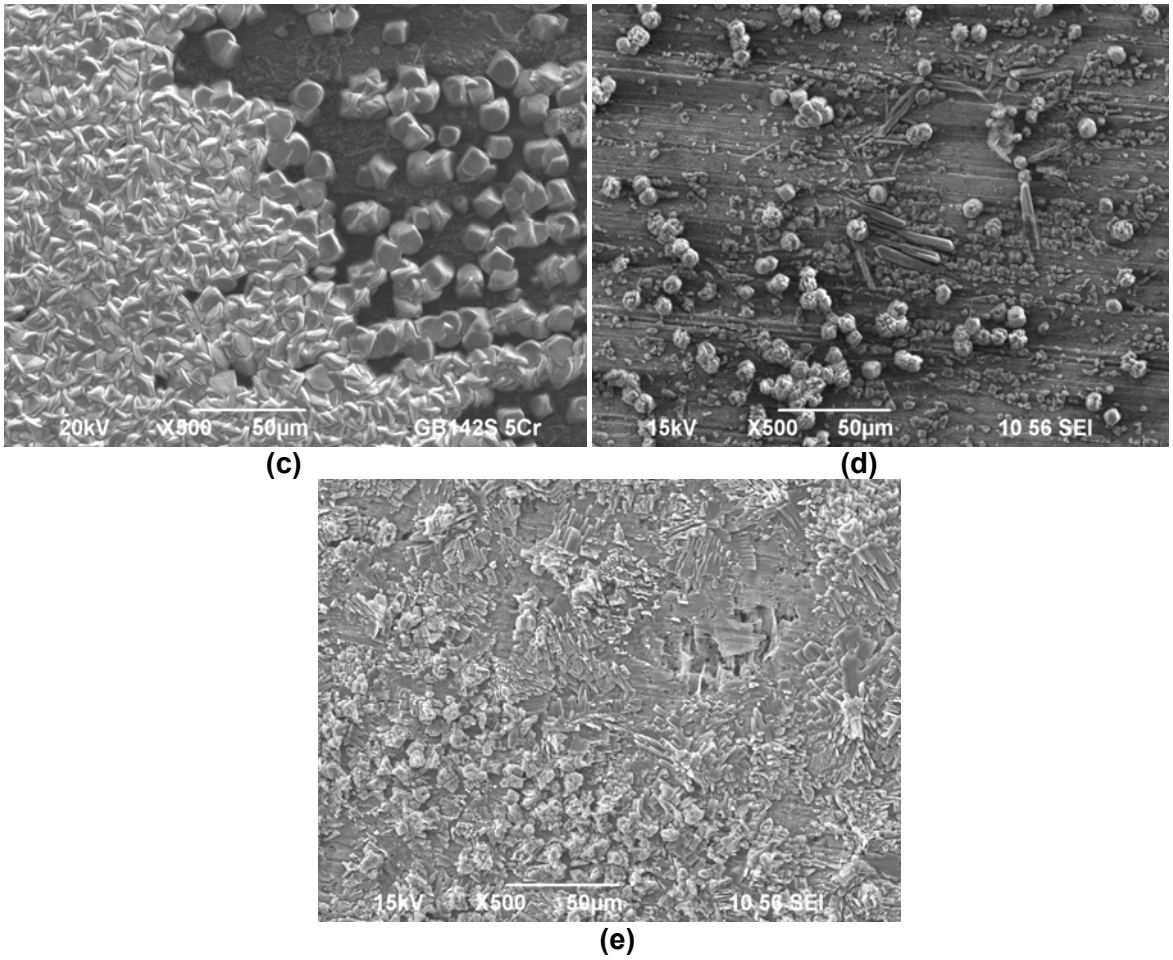

Figure 4: SEM images of recovered samples (G10180) from experiments conducted at 80°C and pCO_2 of 0.05 MPa with 10ppm Fe^{2+} for (a) 0ppm Ca^{2+}, (b) 10ppm Ca^{2+}, (c) 100ppm Ca^{2+}, (d) 1,000ppm Ca^{2+} and (e) 10,000ppm Ca^{2+}.

Figure 5 represents the XRD data of specimens tested with 0 ppm Ca^{2+}, 10 ppm Ca^{2+}, 100 ppm Ca^{2+}, 1,000 ppm Ca^{2+} and 10,000 ppm Ca^{2+}. The XRD data in Figure 5 (a) confirms the presence of $FeCO_3$ on the surface. In Figure 5 (b), based on the XRD data, it can be concluded that a thick and protective layer was formed on the surface, as the main peak of α-Fe related to diffraction from the steel substrate cannot be detected. The XRD data shows less intense, broadened and shifted peaks as a result of the substitution of the larger Ca^{2+} for Fe^{2+} in the $FeCO_3$ structure. This results in formation of a solid solution with the formula $Fe_xCa_yCO_3$ (x + y = 1). According to Figure 5 (c), similar to the experiment condition #2 with the addition of 10ppm Ca^{2+}, the XRD data again shows broadened and shifted peaks relative to $FeCO_3$ with their more profound differences, compared with Figure 5 (b), being due to the higher concentration of Ca^{2+} in the electrolyte. Consequently, this is a consequence of greater substitution of Fe^{2+} with Ca^{2+} during formation of the solid solution; compositional complexity and concentration gradients within the $Fe_xCa_yCO_3$ scale is reflected by significant asymmetry in the principle diffraction peaks between 30-32 2θ. The XRD data shown in Figure 5 (d) is indicative of a transition to a physical mixture of $CaCO_3$ with a solid solution of $Fe_xCa_yCO_3$ on the steel surface. The high corrosion rate in this experiment may be the result of the formation of mostly $CaCO_3$ rather than $FeCO_3$ or $Fe_xCa_yCO_3$ on the surface. This would indicate that $CaCO_3$ is not as protective as $FeCO_3$ or $Fe_xCa_yCO_3$. According to the XRD data shown in Figure 5 (e), there is a physical mixture of the $CaCO_3$ and a solid solution of $Fe_xCa_yCO_3$ on the surface. The high corrosion rate in this experiment is likely the result of the formation of mostly $Fe_xCa_yCO_3$ with a high concentration of Ca^{2+} on the steel surface.

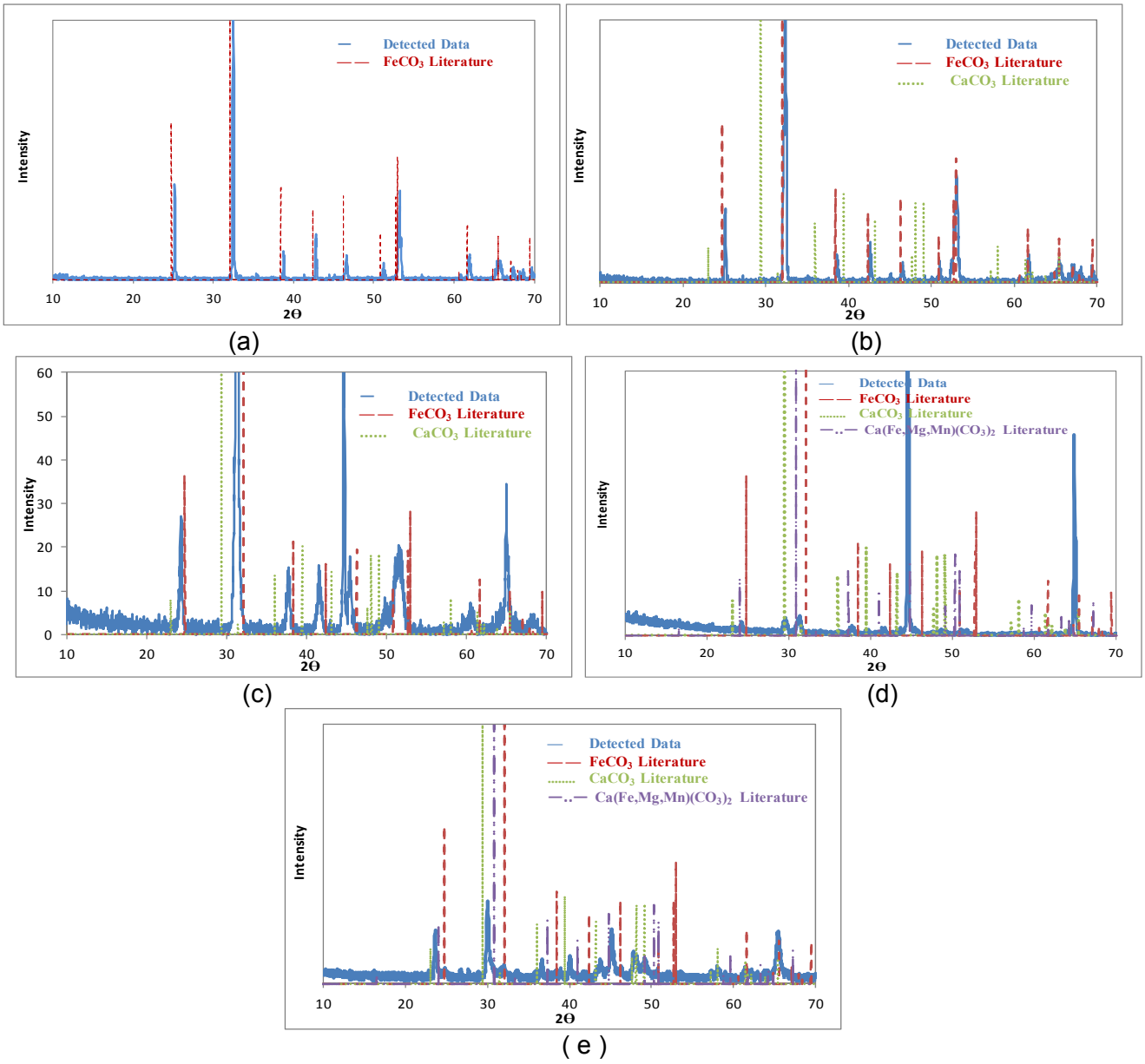

Figure 5: XRD data of recovered samples (G10180) from experiments conducted at 80°C and pCO_2 0.05 MPa with 10ppm Fe^{2+} (a) 0ppm Ca^{2+}, (b) 10ppm Ca^{2+}, (c) 100ppm Ca^{2+}, (d) 1,000ppm Ca^{2+} and (e) 10,000ppm Ca^{2+}.

Figure 6 shows the cross section analysis of the tested conditions with 0, 10, 1,000 and 10,000 ppm Ca^{2+} (note that the cross section from the 100 ppm Ca^{2+} experiment was not available). As is shown in Figure 7 (a) and (b), there is not a significant difference in the layer on the surface between 0 and 10 ppm Ca^{2+}. On the other hand, in the presence of 1,000ppm Ca^{2+} two different layers on the steel surface were detected. According to the EDS line graph in Figure 7 (c), the concentration of Fe in the layer immediately adjacent to the steel surface is higher than for Ca whereas the layer on the outer surface has the opposite relationship. Recall that the XRD data shows two distinct phases: $Fe_xCa_yCO_3$ and $CaCO_3$. Taken in conjunction with the cross-section analysis, this would imply that a bilayer structure had formed with $CaCO_3$ scale growing from the surface of the $Fe_xCa_yCO_3$ corrosion product. Figure 7 (d), the cross section analysis of the experiment with 10,000 ppm Ca^{2+}, does not show an obvious bilayer structure at the steel surface. There is, however, a significant Ca/Fe concentration

gradient, consistent with the XRD data. There seems to be an increased "roughening" of the steel surface as the Ca^{2+} concentration increases, however this is better seen in the images below taken after the surface layer was removed.

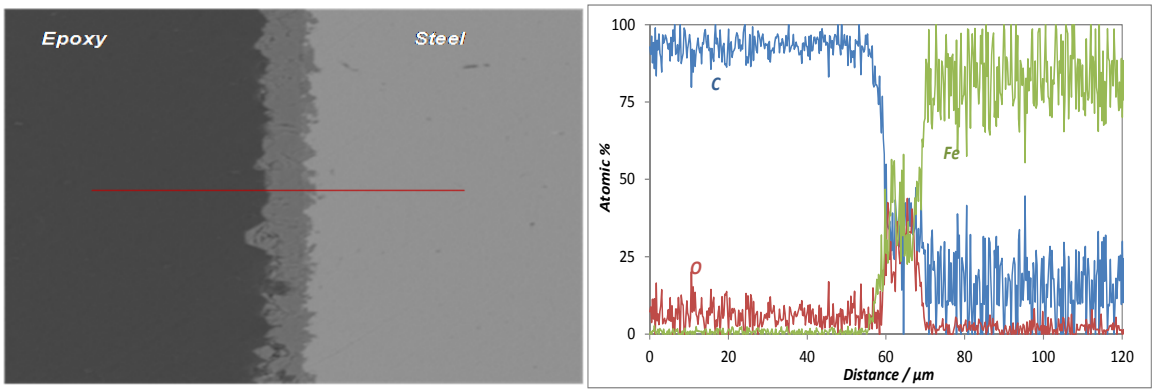

(a)

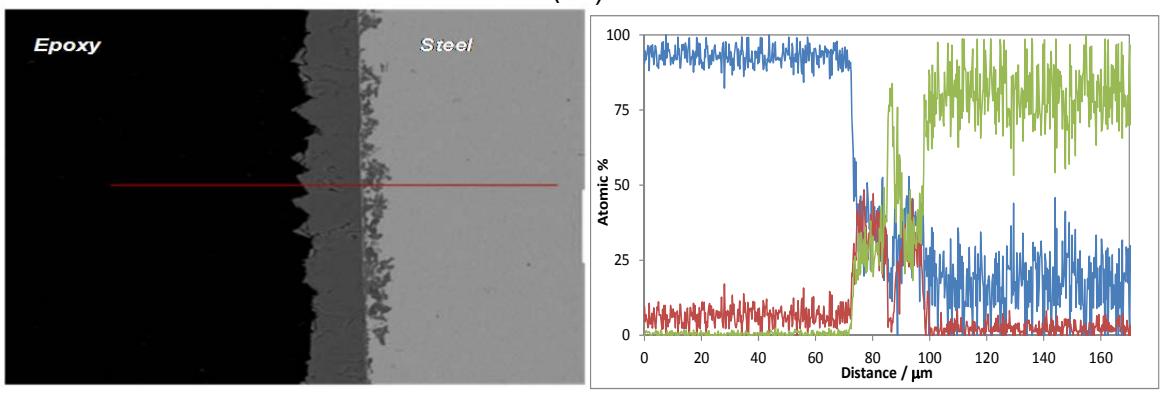

(b)

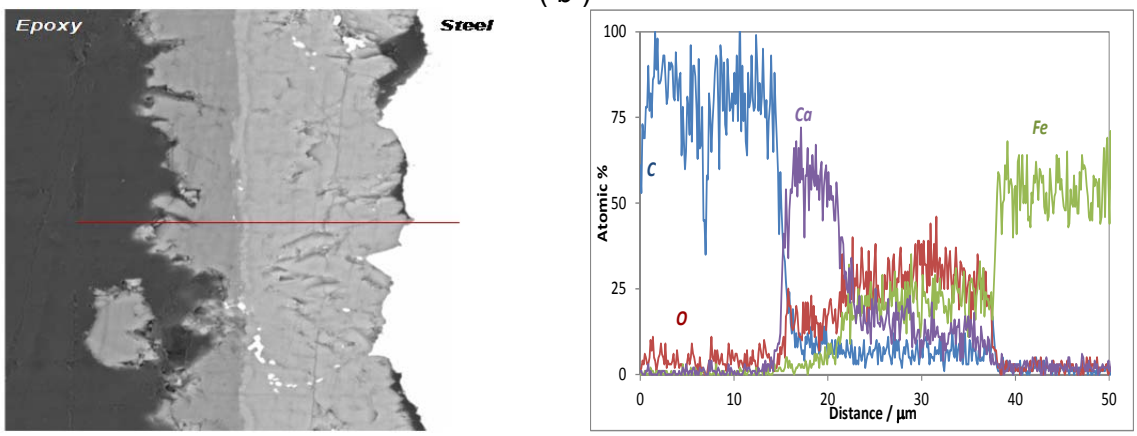

(c)

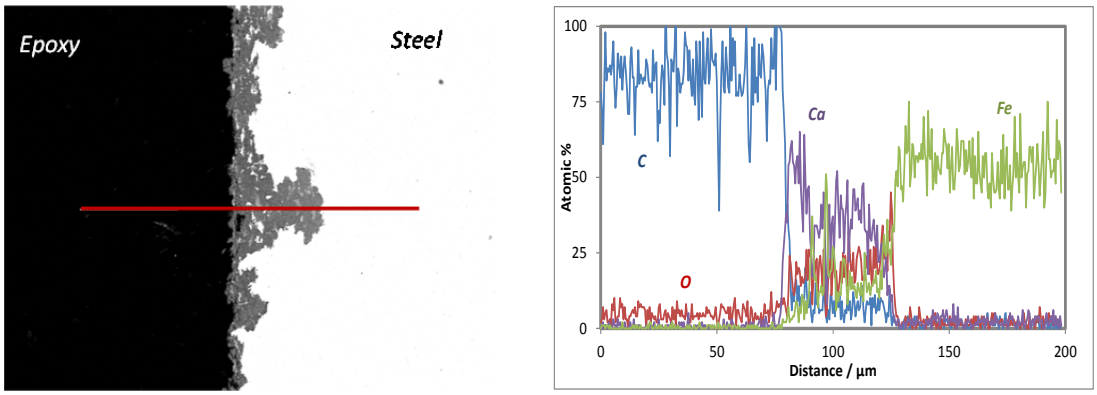

(d)

Figure 6: Cross section image and EDS spectra of samples (G10180) recovered from experiments at 80°C and pCO_2 0.05 MPa with 10ppm Fe^{2+} and (a) 0ppm Ca^{2+}, (b) 10 ppm Ca^{2+}, (c) 1,000ppm Ca^{2+} and (d) 10,000ppm Ca^{2+}.

Figure 7 shows SEM images of the surface after specimens were treated with Clarke solution which completely removed the surface layer. General roughening of the surface is confirmed, as the Ca^{2+} concentration is increased. At the highest Ca^{2+} concentration of 10,000 ppm there appears to be some initiation of pitting, however this is difficult to judge due to the relatively short duration of the experiments. The calculated maximum penetration rate, according to deepest pit found by the IFM analysis is 6.0 mm/yr, as shown in Figure 8. This is significantly higher than the average uniform corrosion rate detected by LPR, see Figure 1 (a).

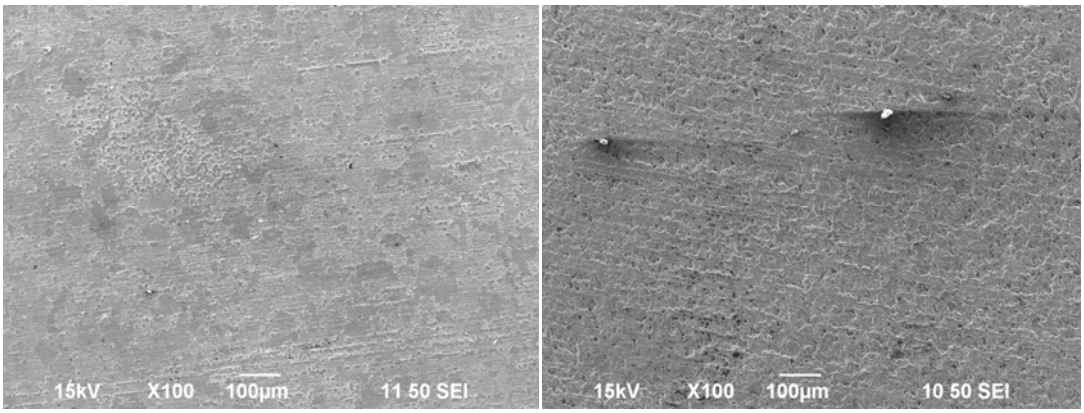

(a) (b)

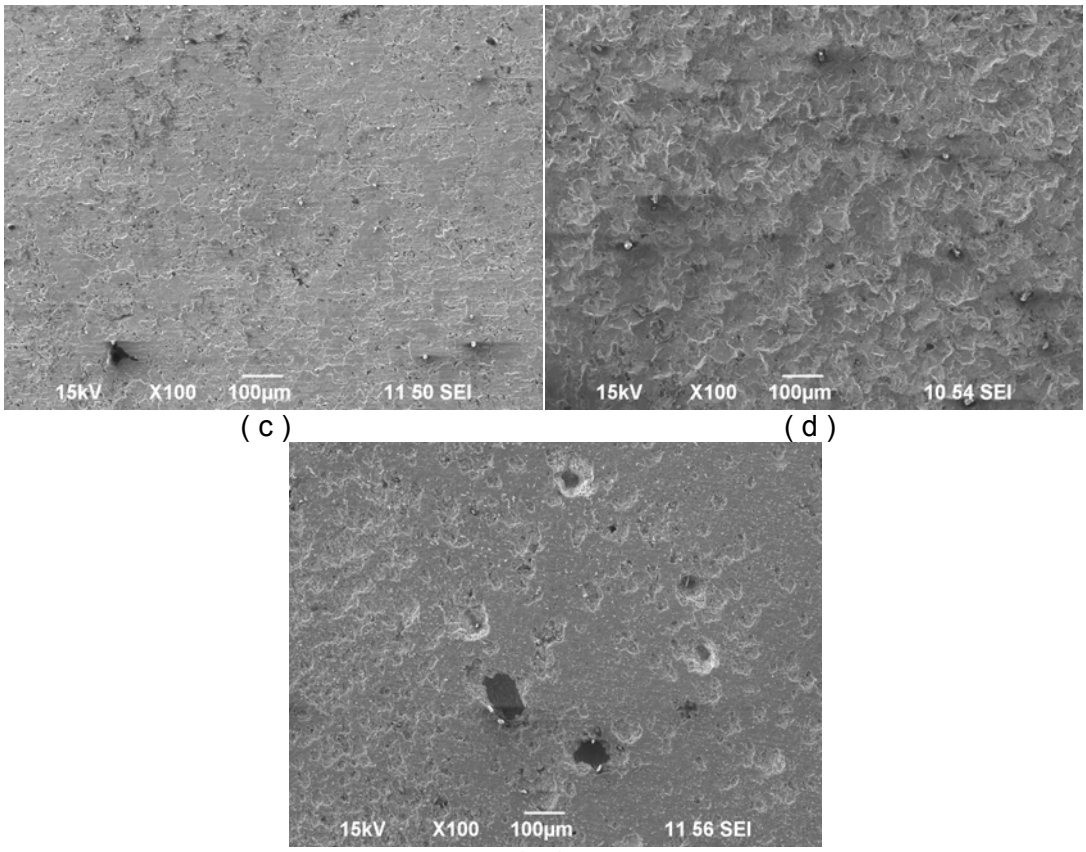

Figure 7: Surfaces after corrosion product removal from samples (G10180) for experiments conducted at 80◦C and pCO_2 0.05 MPa with 10ppm Fe2+ and (a) 0ppm Ca^{2+}, (b) 10ppm Ca^{2+}, (c) 100ppm Ca^{2+}, (d) 1,000ppm Ca^{2+} and (e) 10,000ppm Ca^{2+}.

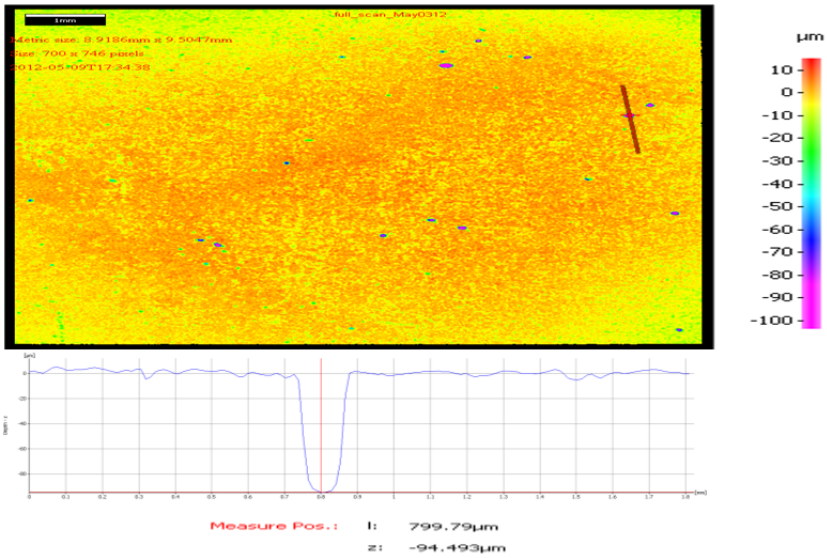

Figure 8: IFM of sample (G10180) after removal of corrosion product for the experiment conducted at 80◦C and pCO_2 0.05 MPa with 10ppm Fe^{2+} + 10,000ppm Ca^{2+}

CONCLUSIONS

It can be concluded that:

- The presence Ca^{2+} affected the corrosion behavior by changing the water chemistry, particularly as the formation of non-protective $CaCO_3$ interfered with formation of protective $FeCO_3$.
- The low Ca^{2+} concentration (<100ppm) did not significantly affect the corrosion rate.
- At high concentration of Ca^{2+} (≥1,000ppm) the corrosion behavior was different and high corrosion rates were observed.

ACKNOWLEDGMENTS

The authors would like to thank Bruce Brown for his support in this study. The financial support of the Department of Chemical and Biomolecular Engineering is appreciated.

REFERENCES

1. A. Pfennig, A. Kranzmann “Reliability of pipe steels with different amounts of C and Cr during onshore carbon dioxide injection” Green Gas Control, 5 (2011): p. 757–769.

2. J. Gale, J. Davison “Transmission of CO_2—safety and economic considerations” Energy, 29(2004), pp. 1319–1328.

3. Z. Xian, X. Ming, L. Hong, and H. Yong , “Formation Characteristic of CO_2 Corrosion Product Layer of P110 Steel Investigated by SEM and Electrochemical Techniques,” Journal of Iron and Steel Research, International, 16(2009), pp. 89–94.

4. Z. Xian, L. Ping, H. Ming, L. Hong, and L. Lin, “Effect of Ca^{2+} and Mg^{2+} on CO_2 corrosion behavior of tube steel,” J. Iron. Steel Res. Int.,12 (2005), p. 38-42 .

5. C. Ding, K. Gao, and C. Chen “ Effect of Ca^{2+} on CO_2 corrosion properties of X65 pipeline steel,” Int. J. Miner. Metall. Mater,16 (2009) p. 661-666.

6. X. Jiang, Y.G. Zheng, D.R. Qu and W. Ke, “Effect of calcium ions on pitting corrosion and inhibition performance in CO_2 corrosion of N80 steel,” Corrosion Science, 48 (2006) p. 3091-3108.

7. C. Ren, X. Wang, L. Liu, H. Yang, and N. Xian, “Lab and field investigations on localized corrosion of casing,” Materials and Corrosion, 63 (2012) , pp. 168–172.

8. S. Zhu, J. Wei, Z. Bai, G. Zhou, J. Miao, and R. Cai, “Failure analysis of P110 tubing string in the ultra-deep oil well,” Engineering Failure Analysis, 18 (2011) , pp. 950–962.

9. K. Gao, F. Yu, X. Pang, G. Zhang, L. Qiao, W. Chu, and M. Lu, “Mechanical properties of CO_2 corrosion product scales and their relationship to corrosion rates,” Corrosion Science, 50 (2008), pp. 2796–2803.

10. ASTM G1, “Standard practice for preparing, cleaning, and evaluating corrosion test specimens” (West Conshohocken, PA: ASTM).

11. S. Nešić, “Key issues related to modeling of internal corrosion of oil and gas pipelines – A review,” Corrosion Science, 49(2007), pp. 4308–4338.

12. S. Nešić, M. Nordsveen, R. Nyborg, A. Stangeland, “A mechanistic model for carbon dioxide corrosion of mild steel in the presence of protective iron carbonate films — Part 2: A numerical experiment,” 59 (2003), pp. 489–497.

13. S. Nešić, Carbon Dioxide Corrosion of Mild Steel (2011), R. Winston Revie, Uhlig’s Corrosion Handbook, 3rd ed., Hoboken, NJ, pp.229-245

14. W. Sun and S. Nešić, “Basics revisited: kinetics of iron carbonate scale precipitation in CO_2 corrosion”, paper no. 06365 (Houston, TX: NACE, 2006).

15. L. Plummer, E. Busenberg, “The solubilities of calcite, aragonite and vaterite in CO_2-H_2O solutions between 0 and 90°C, and an evaluation of the aqueous model for the system $CaCO_3$-CO_2-H_2O” Geochimica et Cosmochimica Acta, 46(1982), pp1011-1040.

16. J.E. Wajon, G. Ho, and P.J. Murphy “Rate of precipitation of ferrous iron and formation of mixed iron-calcium carbonates by naturally occurring carbonate materials,” Water Res, 19 (1985) p. 831-837.